# Visualizing Ricci Flow of Manifolds of Revolution

J. Hyam Rubinstein and Robert Sinclair

Department of Mathematics & Statistics

The University of Melbourne

Parkville

Victoria 3010

Australia

February 1, 2008

## Abstract

We present numerical visualizations of Ricci Flow of surfaces and 3-dimensional manifolds of revolution. `Ricci_rot` is an educational tool which visualizes surfaces of revolution moving under Ricci flow. That these surfaces tend to remain embedded in $\mathbb{R}^3$ is what makes direct visualization possible. The numerical lessons gained in developing this tool may be applicable to numerical simulation of Ricci flow of other surfaces. Similarly for simple 3-dimensional manifolds like the 3-sphere, with a metric which is invariant under the action of $SO(3)$ with 2-sphere orbits, the metric can be represented by a 2-sphere of revolution, where the distance to the axis of revolution represents the radius of a 2-sphere orbit. Hence we can also visualize the behaviour of such a metric under Ricci flow. We discuss briefly why surfaces and 3-manifolds of revolution remain embedded in $\mathbb{R}^3$ and $\mathbb{R}^4$ respectively, under Ricci flow and finally indulge in some speculation about the idea of Ricci flow in the larger space of positive definite and indefinite metrics.

## 1 Introduction

Understanding Ricci flow has become fundamental to attempts to prove Thurston's geometrization conjecture ([5], [8], [18], [19]). Since Ricci flow is geometric by nature, it is natural to ask whether it can be visualized. Unlike mean-curvature and related flows, which act in the first instance as a force pushing on a surface and therefore tend to keep surfaces embedded in Euclidean space, Ricci flow acts directly on the metric of the surface, tending not to preserve embeddedness. A number of interesting results have been obtained by restricting to classes of metrics of revolution, since such symmetries are preserved under Ricci flow and the metric depends on considerably fewer parameters in such cases ([21], [2], [13]). We will discuss for this class of metrics, why Ricci flow does preserve embeddedness in Euclidean space ([9]). Moreover, the key phenomenon of neck pinching occurs

naturally for metrics of revolution. Good estimates are available to understand the limiting behaviour of metrics as they become singular under neck pinching in ([21], [2]). Our visualization approach enables us to generate interesting pictures and information about neck pinching. In [7], it is shown that any metric on the 2-sphere converges to the round metric under Ricci flow, so neck pinching occurs only in higher dimensions.

Note that there are many interesting questions about Ricci flow for 3-dimensional manifolds. There are a limited number of examples where one knows completely how the metric evolves ([8]). It would be very useful to have further examples where Ricci flow continues for infinite time, without developing singularities. For example, there are important constructions (Dehn surgery) of metrics with strictly negative sectional curvature on 3-manifolds ([11], [3]). But even in this case, it is not clear whether singularities will form under Ricci flow. In fact, no examples are known where a metric with all sectional curvatures negative flows to a metric with positive sectional curvature at some points.

# 2  Preserving the Embedding into Euclidean Space

In this section, we give a quick discussion of why $n$-dimensional spheres of revolution ($K_2 = 1$ – see Section 5.1), which are initially isometrically embedded into Euclidean $(n+1)$-dimensional space, remain isometrically embedded, so long as Ricci flow has a smooth solution.

## 2.1  Characterising when Isometric Embeddings exist

We observe a simple extension of [9]. Note that in later sections, we will use extrinsic coordinates, which are useful to see how points of the surface or manifold move under Ricci flow when visualized in Euclidean space. Here it is more convenient to use intrinsic coordinates. So on $S^n$, a metric is chosen of the form $ds^2 + \alpha^2(s)d\theta^2$, where $s$ is arc length along a geodesic joining the North Pole to the South Pole and $\theta$ represents the coordinates in a hypersphere of radius $\alpha(s)$, which is the orbit of an isometric action of $SO(n)$ on $S^n$, where the orbit space is an arc. We assume that $s$ varies between 0 and $L$.

In [9], it is shown that a necessary and sufficient condition that $S^2$, with a metric of this form, can be isometrically embedded in $\mathbb{R}^3$ as a surface of revolution, is that the integral of Gaussian curvature over any "polar cap" is positive, where such a region consists of all points where either $0 \leq s \leq k$ or $k \leq s \leq L$, for some $k$ with $0 < k < L$. Note also that a surface of revolution in $\mathbb{R}^3$ is invariant under an isometric action of $SO(2)$ by rotation about the $x^1$ axis. Similarly we define a manifold of revolution in $\mathbb{R}^{(n+1)}$ as being invariant under the isometric action of $SO(n)$ by rotation about the $x^1$ axis. Finally we follow [9], by requiring that any manifold of revolution $\mathbb{R}^{(n+1)}$ has at most one component of intersection with any hyperplane of the form $x^1 = k$ for any constant $k$. Equivalently, the manifold is obtained by rotating the graph of a function of one variable around the $x^1$ axis, by the action of $SO(n)$. Note that for visualization purposes, it is not essential but is certainly convenient to have this restriction.

**Theorem 1** *Suppose that a metric of the form $ds^2 + \alpha^2(s)d\theta^2$ is chosen on $S^n$. Then there is an isometric embedding as a manifold of revolution in $\mathbb{R}^{(n+1)}$ if and only if the same metric, viewed as on $S^2$, can be isometrically embedded into $\mathbb{R}^3$ as a surface of revolution.*

The proof of this theorem is very easy and is left to the reader.

## 2.2 Ricci Flow preserves Embeddability of Manifolds of Revolution

An observation about the characterisation in [9] is as follows. For a polar cap, Gauss Bonnet shows that the sum of the integral of the Gaussian curvature of the cap and the integral of the curvature of the boundary curve $C$ is $\pi$. Therefore positivity of the first integral is equivalent to the second integral being strictly less than $\pi$. Note that $C$ is the orbit of $SO(2)$ acting on a plane parallel to the $x^2x^3$ plane and so is a standard round circle in this plane, with centre on the intersection of the plane with the $x^1$ axis. Hence the integral of its curvature in $\mathbb{R}^3$ is exactly $\pi$ and the direction of its curvature at each point points towards the $x^1$ axis. But then to compute the curvature in the surface of revolution, one has to project onto the tangent space of this surface. Hence the projected curvature vector will be shorter, unless the tangent plane is vertical at every point of $C$. So this shows that the condition on the polar caps remains true as Ricci flow proceeds, unless at some time and for some value of $s$, with $0 < s < L$, $|\alpha'(s)| = 1$. Therefore we need to show that $|\alpha'(s)| < 1$ remains true, away from the poles, so long as Ricci flow produces a smooth solution ([2],[9],[13]), to prove the following result.

**Theorem 2** *If there is an isometric embedding of $S^n$ as a manifold of revolution in $\mathbb{R}^{(n+1)}$ then the manifold remains isometrically embedded so long as Ricci flow gives a smooth solution.*

**Proof** Let $v = \alpha'$, where $v$ and $\alpha$ are viewed as functions of $s$ and time $t$, and as above, the derivative of $\alpha$ is taken with respect to $s$. By equation (16) of [2], $v$ satisfies the following evolution equation.

$$\partial_t v = v_{ss} + \frac{n-2}{\alpha} vv_s + \frac{n-1}{\alpha^2}(1 - v^2)v.$$

Here we are using $v_s$ to denote partial differentiation in the $s$ variable.

Now initially, $|v| = |\alpha_s| < 1$ for all values $0 < s < L$, by assumption. Let $t$ be a first value of time for which $|v(s,t)| = 1$, at some $s$ not corresponding to the North or South pole of the sphere. If $v(s,t) = 1$, then this is a maximum value of $\alpha$ whereas if $v(s,t) = -1$, then this is a minimum value.

So we see by the maximum principle, (see eg [8]) that this gives a contradiction, since $1 - v^2 = v_s = 0$ for both cases. This shows that the sphere does remain embedded, so long as it is smooth.

3

# 3 Computational Formulation

A two-dimensional surface of revolution of genus zero embedded in $\mathbb{R}^3$ can be defined in a polar representation with coordinates $x^1 = \rho$ and $x^2 = \theta \in [0, 2\pi[$ by a metric of the form

$$[g_{\mu\nu}] = \begin{bmatrix} h(\rho) & 0 \\ 0 & m(\rho) \end{bmatrix},$$

where $\sqrt{m(\rho)}$ has the direct physical interpretation as the radius from the axis of rotation. For a closed surface, we require

$$m(\rho_{pole}) = 0.$$

We have chosen $\rho_{\text{North\_Pole}} = 0$ and $\rho_{\text{South\_Pole}} = \pi$. When $h(\rho)$ is a constant, $\sqrt{h} \times \rho$ is the distance of a point with coordinates $(\rho, \theta)$ from the North Pole along a meridian. Smoothness at the poles demands

$$\left. \frac{\partial \sqrt{m(\rho)}}{\partial \rho} \right|_{\rho = \rho_{pole}} = \sqrt{h(\rho_{pole})}, \qquad \rho_{pole} \in \{0, \pi\}. \tag{1}$$

Note that the necessary and sufficient condition for isometric embeddability as a classical surface of revolution in $\mathbb{E}^3$ for $S^1$-invariant metrics on $S^2$ – the nonnegativity of the integrals of the curvature over all disks centred at a pole – is given in [9]. The generating curve (cross-section) of the surface of revolution is given by

$$x(\rho) = \int_0^\rho \sqrt{h(s) - \left( \frac{\partial \sqrt{m(s)}}{\partial s} \right)^2} \, ds$$

$$y(\rho) = \sqrt{m(\rho)} \tag{2}$$

with $\rho \in [0, \pi]$.

The Ricci tensor is

$$[R_{\mu\nu}] = \begin{cases} \begin{bmatrix} \dfrac{(m')^2}{4m^2} - \dfrac{m''}{2m} + \dfrac{m' h'}{4m h} & 0 \\ 0 & \dfrac{(m')^2}{4m h} - \dfrac{m''}{2h} + \dfrac{m' h'}{4h^2} \end{bmatrix} & (\rho \in ]0, \pi[) \\[2em] \begin{bmatrix} \dfrac{m''''}{4m''} - \dfrac{h''}{2h} & 0 \\ 0 & 0 \end{bmatrix} & (\rho \in \{0, \pi\}), \end{cases} \tag{3}$$

where primes denote partial differentiation with respect to $\rho$.

Ricci flow satisfies

$$\frac{\partial g_{\mu\nu}}{\partial t} = -2R_{\mu\nu}.$$

4

The possible initial metrics `Ricci_rot` provides are given by

$$\begin{bmatrix} 1 & 0 \\ 0 & \left(\dfrac{\sin\rho + c_3 \sin 3\rho + c_5 \sin 5\rho}{1 + 3c_3 + 5c_5}\right)^2 \end{bmatrix}. \tag{4}$$

These surfaces are symmetric under reflections about a plane normal to their axis of rotation which passes through their centre of mass. This extra symmetry has proven useful in making the simulation faster, since it then suffices to compute on only half of the surface.

Attempting to integrate using Equation (3) and central finite differences in a purely explicit scheme leads, not surprisingly to numerical instability, particularly (but not only) at the poles. This instability can be reduced significantly by noting that

$$\frac{(m')^2}{4m^2} - \frac{m''}{2m} = \frac{-(\sqrt{m})''}{\sqrt{m}}.$$

## 3.1 Filtering and Reparametrization

The numerical instabilities are however persistent enough to require more potent measures. We did not try any implicit scheme, which may have alleviated the numerical instabilities, but would still have required very small time steps near the poles.

Inspired by spectral methods [4], we first introduced a filter which consists of transforming to Fourier space (DFT), dropping shorter wavelength terms, and then transforming back. This process is facilitated by noting that the rotational and reflection symmetries of the family of surfaces (4) are preserved by Ricci flow. We can therefore write

$$h(\rho) = \sum_{i=0}^{N_h} h_i \cos 2i\rho$$

and

$$\sqrt{m(\rho)} = \sum_{i=0}^{N_m} m_i \sin\left((2i+1)\rho\right),$$

where equality of course only applies to $N_h = N_m = \infty$. We actually choose $N_h$ and $N_m$ to be much less than the number of points used in the finite difference scheme, and find that there is no need to implement the FFT. We need to ensure that (1) is satisfied at the poles, to be sure that the generating curve (2) can be found. We do this by multiplying the computed values of $\sqrt{m}$ by

$$\frac{\dfrac{\sqrt{h(\rho_{pole})}}{\sum_{i=0}^{N_m}(2i+1)\times m_i} + K\left(\rho - \rho_{pole}\right)^2}{1 + K\left(\rho - \rho_{pole}\right)^2},$$

5

where $K$ is a small positive constant, but large enough that this correction factor quickly becomes unity away from the poles. Setting $K = 0$ has the unwanted side-effect that local numerical errors near the poles can lead to global changes in shape which do not satisfy the Ricci flow.

By its very nature, the Ricci flow forces some parts of a surface to contract while others expand. This means that whatever set of nodes we have chosen for our finite-difference scheme will effectively become less and less evenly distributed, creating further sources of numerical instability where they become too dense. The solution to this problem is to recall that any given surface corresponds to many different parametrizations, each with a corresponding metric. From a numerical point of view, the most pleasant parametrizations let $h(\rho)$ be a constant (this corresponds to $\rho$ being directly proportional to distance from a pole). Let

$$\ell(\rho) = \int\limits_{s=0}^{\rho} \sqrt{h(s)}\, ds$$

be the distance from the North Pole. We have the freedom to reparametrize:

$$[g_{\mu\nu}] = \left[ \begin{array}{cc} h(\rho) & 0 \\ 0 & m(\rho) \end{array} \right] \mapsto \left[ \begin{array}{cc} \left(\dfrac{\ell(\pi)}{\pi}\right)^2 & 0 \\ 0 & m\left(\ell^{-1}\left(\dfrac{\rho \times \ell(\pi)}{\pi}\right)\right) \end{array} \right]$$

where $\rho \in [0, \pi]$ both before and after. It is this reparametrization which, performed after every few iterations of the explicit integration and filtering steps, has made `Ricci_rot` stable enough to use.

# 4    Use of the Software

First, a quick introduction: Press "`n`" and then drag the mouse to choose an initial surface. Then hold down the up-arrow key to watch the flow until it stops. Once one has begun flowing, dragging the mouse will rotate the surface.

## 4.1    Details

`Ricci_rot` is an ANSI C program [15] which uses the OpenGL standard [17] to display graphics. It should therefore be portable, although it has only been tested on a Mac OS X platform.

Upon launch, a window is opened with the image of a sphere with blue meridians and parallels. This initial shape can be deformed by holding down the left mouse button and dragging in any direction. The possible initial shapes belong to the family (4), where $c_3$ is varied by horizontal, and $c_5$ by vertical motion. The program will not accept all possible values of $c_3$ and $c_5$, so, dragging very far in any direction, one may find that the shape ceases changing.

To examine the shape, pressing "f" (for "flow") will put the program into flow mode. The meridians and parallels change colour. Now, dragging the mouse rotates the surface. To make any more changes, pressing "n" (for "new shape") will put the program back in its initial mode. The meridians and parallels change colour back to blue, and dragging the mouse changes the shape.

When one has chosen a shape one wishes to flow, it is enough to begin pressing the up-arrow key. Usually this key will repeat if held down. Then one can see the surface flow continuously. Since the program is now in flow mode, dragging the mouse will rotate the surface.

Once the program has met with a numerical instability, the flow will stop, and the parallels and meridians will appear black. Any ripples which may appear on the surface at this stage are a result of the numerical instability.

At any time, pressing the left-arrow or right-arrow keys will rotate the surface anti-clockwise or clockwise respectively.

The down-arrow key flows the surface backwards in time. This evolution is highly unstable. One should not expect to be able to flow for very long.

Pressing "m" at any stage will change the display mode from showing the surface to showing the components of the metric ($g_{11} = h$ in green and $g_{22} = m$ in blue) and the surface's cross-section in white. To revert to displaying the surface in $\mathbb{E}^3$, press "s".

There is a bright spotlight. This can be turned on or off by pressing the right mouse button. A menu will appear, from which one can choose to turn the spotlight on or off (or change to and from "flow" and "new shape" modes). It can be rotated (in a rather non-intuitive way) by dragging the mouse with the middle mouse button held down.

## 4.2   Examples

The first example is of a dumbbell shape, given by Equation (4) with $c_3 = 0.766$ and $c_5 = -0.091$. This surface's flow is illustrated in Figure 1 with time step $dt = 0.01$. The flow of its cross-section is provided in Figure 2 time step $dt = 0.002$. It is interesting to compare this with Figure 4 of [6], which is an illustration of the mean-curvature flow of the cross-section of what is initially a dumbbell shape.

Figures 3, 4, 5 and 6 were all generated using the initial surface given by $c_3 = 0.021$ and $c_5 = 0.598$, and with the time step $dt = 0.002$. The values of $g_{11} = h$ ($h(\rho)$ becomes a constant after reparametrization) are 1, 1.027938, 1.000526, 0.936608, 0.843907, 0.729106, 0.601463, 0.475008, 0.365054, 0.278860, 0.213761 and 0.163754.

The behaviour is in both cases what one expects – flow towards spheres of constant positive Gaussian curvature [7]. See also Chapter 5 of [8], in which it is shown that any solution of the unnormalized Ricci flow on a topological $S^2$ shrinks to a round point in finite time, following [7]. Note that the "modified" Ricci flow in [16], for the special case of surfaces of revolution embedded in Euclidean space, could be visualized in a similar way.
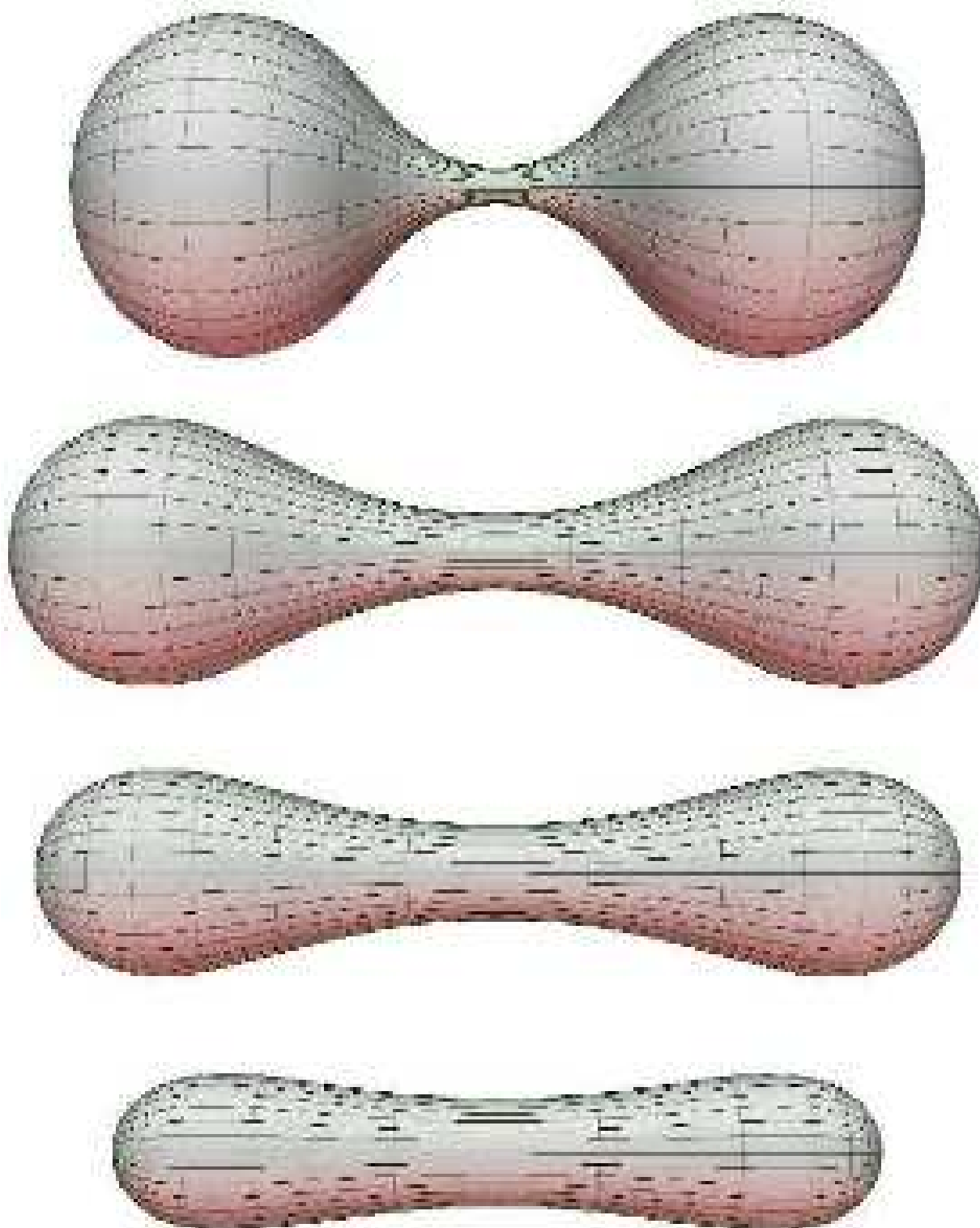
Figure 1: Deformation of a dumbbell-like surface of revolution under Ricci flow. The pictures have been taken at equal time intervals and are drawn to the same scale.
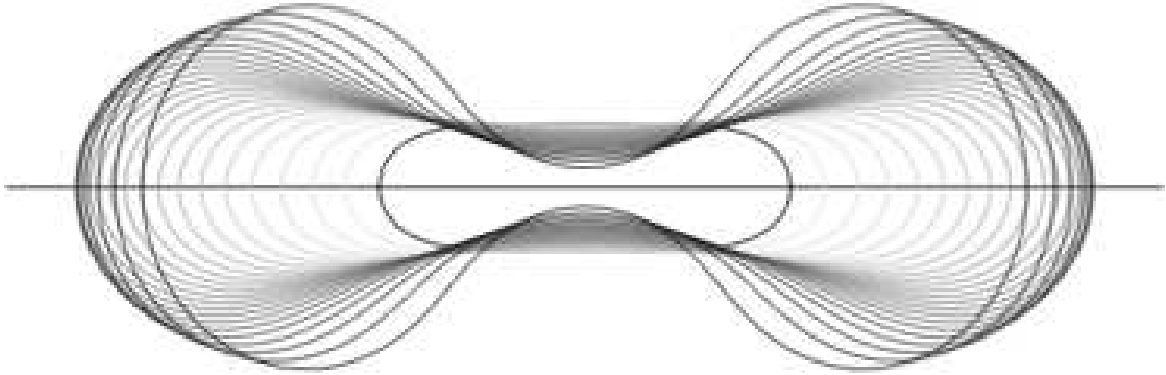
Figure 2: Deformation of the cross-section of a dumbbell surface of revolution under Ricci flow. The axis of rotation is horizontal. The pictures have been taken at equal time intervals. The initial and final curves are both shaded black.

# 5 Three-Dimensional Manifolds of Revolution

## 5.1 A Line cross a Surface of Revolution of Constant Curvature

Let $K_2$ be the Gaussian curvature of a general abstract Riemannian surface of revolution, where $K_2$ is any real constant.

The 3-manifold metric is

$$[g_{\mu\nu}] = \begin{bmatrix} h(\rho) & 0 & 0 \\ 0 & m(\rho) & 0 \\ 0 & 0 & m(\rho)\cos^2\left(\sqrt{K_2}\,\theta\right) \end{bmatrix}, \tag{5}$$

where $\rho \equiv x^1$ plays the role of a latitude and $\theta \equiv x^2$ the role of a latitude on the abstract Riemannian surface of revolution.

The non-zero elements of the Ricci tensor are

$$R_{11} = \frac{(m')^2}{2\,m^2} - \frac{m''}{m} + \frac{m'\,h'}{2\,m\,h} \tag{6}$$

$$R_{22} = \frac{m'\,h'}{4\,h^2} - \frac{m''}{2\,h} + K_2 \tag{7}$$

$$R_{33} = \left(\frac{m'\,h'}{4\,h^2} - \frac{m''}{2\,h} + K_2\right)\cos^2\left(\sqrt{K_2}\,\theta\right), \tag{8}$$

and therefore unnormalized Ricci flow satisfies

$$\frac{\partial h}{\partial t} = \frac{2\,m''}{m} - \frac{(m')^2}{m^2} - \frac{m'\,h'}{m\,h} \tag{9}$$
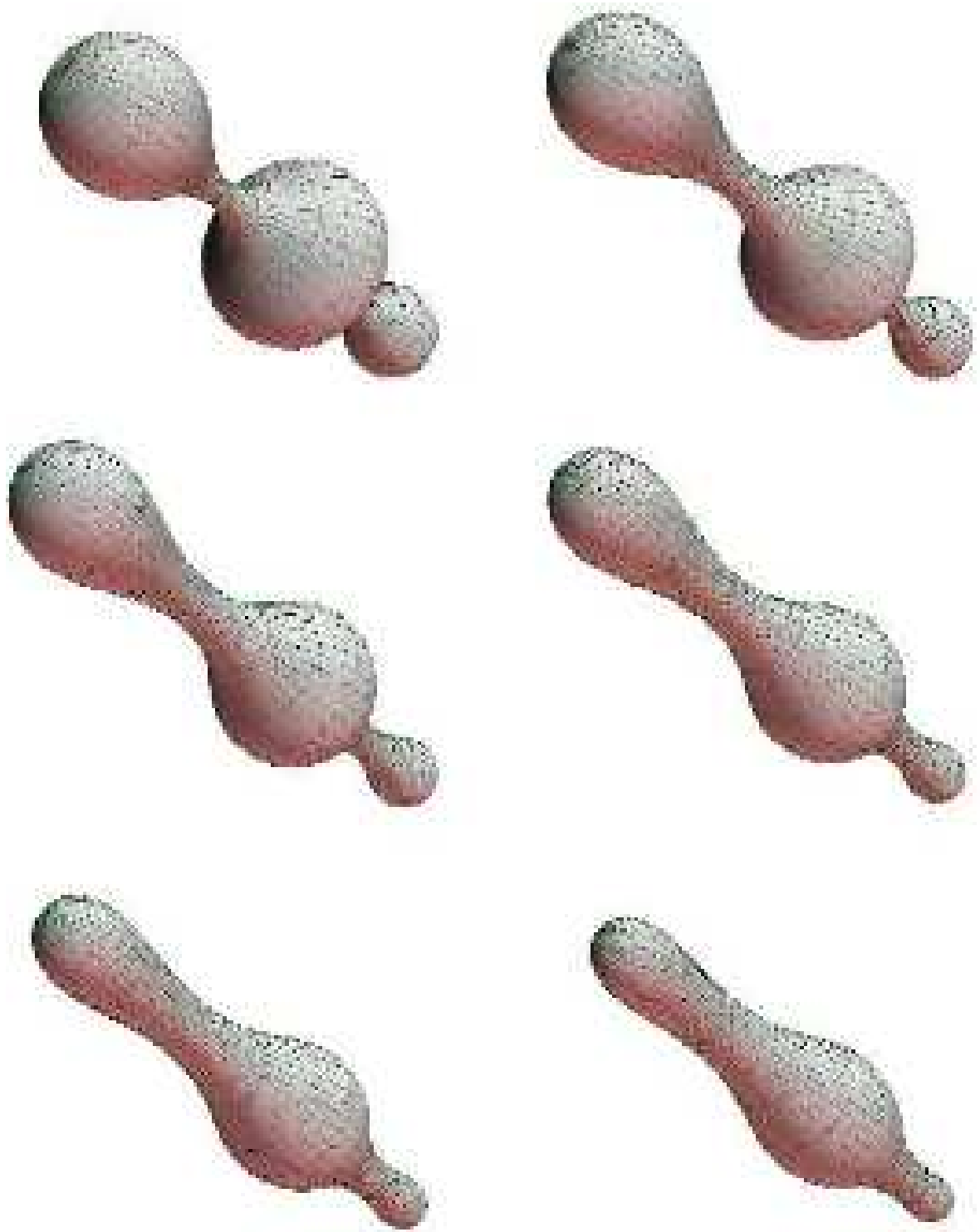
9

Figure 3: Deformation of a surface of revolution under Ricci flow. The pictures have been taken at equal time intervals and are drawn to the same scale. The cross-sections are plotted in Figure 5.
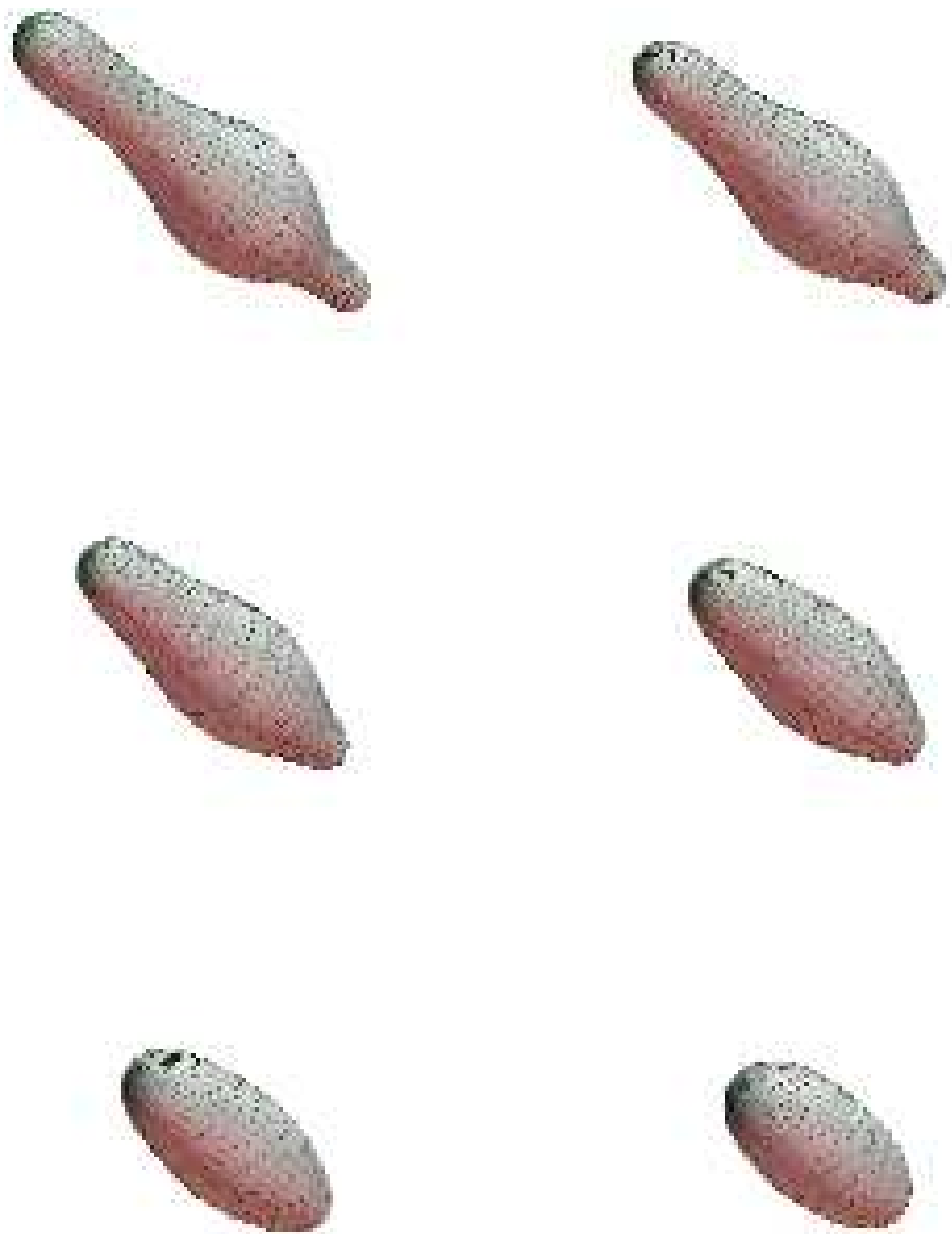
Figure 4: Deformation of a surface of revolution under Ricci flow. The pictures have been taken at equal time intervals and are drawn to the same scale. These pictures are the continuation of the evolution of the surface begun in Figure 3. The cross-sections are plotted in Figure 5.
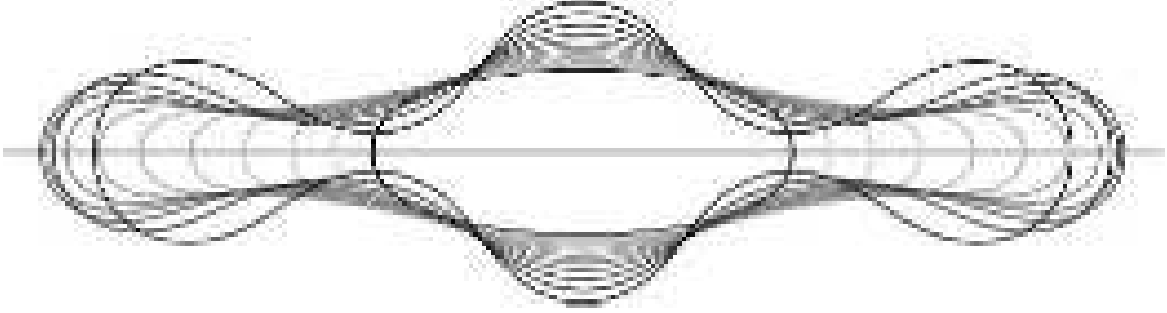
Figure 5: Deformation of the cross-section of a surface of revolution under Ricci flow. The axis of rotation is horizontal. The pictures have been taken at equal time intervals. The initial and final curves are both shaded black.

$$\frac{\partial m}{\partial t} \;=\; \frac{m''}{h} - \frac{m' h'}{2 h^2} - 2 K_2. \tag{10}$$

The scalar curvature is

$$R = \frac{(m')^2}{2 m^2 h} - \frac{2 m''}{m h} + \frac{m' h'}{m h^2} + \frac{2 K_2}{m}. \tag{11}$$

With respect to the mutually orthogonal unit vectors

$$a = \left( \frac{1}{\sqrt{h}}, 0, 0 \right), \quad b = \left( 0, \frac{1}{\sqrt{m}}, 0 \right), \quad \text{and} \quad c = \left( 0, 0, \frac{1}{\sqrt{m} \, \cos \sqrt{K_2}\theta} \right), \tag{12}$$

the sectional curvatures are

$$K(a, b) = K(a, c) = \frac{(m')^2}{4 m^2 h} - \frac{m''}{2 m h} + \frac{m' h'}{4 m h^2} \tag{13}$$

and

$$K(b, c) = \frac{K_2}{m} - \frac{(m')^2}{4 m^2 h}. \tag{14}$$

## 5.2 An Example

We will study the pinching behaviour under unnormalized Ricci flow of the initial 3-manifold with metric given by

$$m(\rho) = \frac{1}{10000} + \sin^2 \left( \frac{9 \pi \rho}{40} \right) \quad h(\rho) = 1 \quad \text{and} \quad K_2 = 1$$

at $t = 0$. We denote the time at which pinching occurs ($m(0) = 0$) by $t = T$.
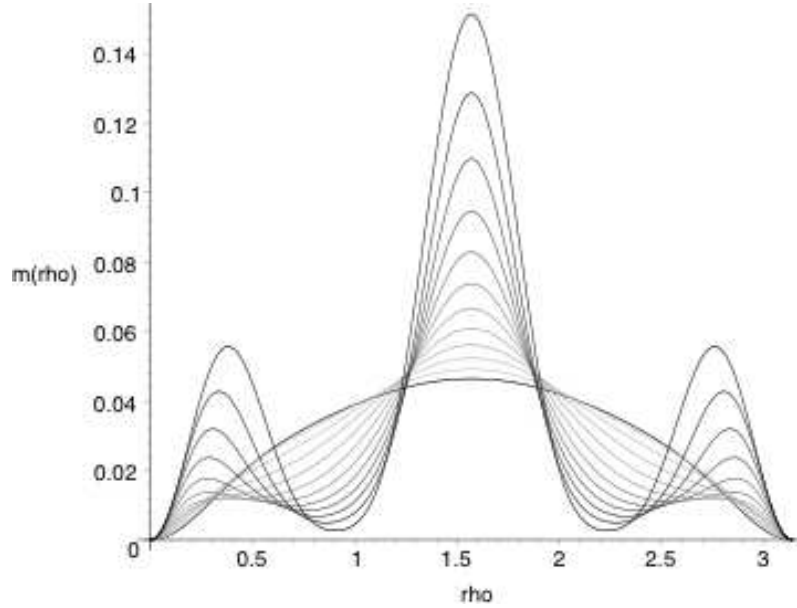
Figure 6: Evolution of the metric component $g_{22} = m(\rho)$ of a surface of revolution under the combined action of Ricci flow and reparametrization – meaning that the corresponding curves $g_{11} = h$ are independent of $\rho$. The curves have been plotted at equal time intervals. The initial and final curves are both shaded black.

### 5.2.1 Qualitative Behaviour

The most direct approach to simulating the flow determined by Equations 9 and 10 is to use an explicit finite-difference formulation. Doing this, we found that the system is (not surprisingly) highly unstable. We identified two modes of instability. One was of a short wavelength – of the type $k \times (-1)^i$ where $i$ is the spatial grid index and $k$ some constant. This type of instability could be removed by simply performing the simulation in Maple [12], using several hundred digits' precision. The other type of instability showed itself as a long-wavelength smooth perturbation which diverged as the number of time-steps was increased. We were not able to eliminate this second source of instability. Practically, it meant that we were restricted to fairly large time-steps. To be more precise, we stepped between $t = 0.000025$, $0.000050$, $0.0000625$, $0.00006875$, $0.000071875$, $0.000075000$, $0.00007578125$, $0.00007656250$, $0.000076953125$ (shown only in Figure 9) and $0.000077343750$. Since we are therefore not able to claim that the method converges to the exact solution, we have chosen to speak of the data from this simulation as being only qualitatively correct.

It is nonetheless informative to consider Figures 7, 8 and 9.

Figures 8 and 9 would suggest that pinching occurs *before* $t = 0.000077343750$. At $t = 0.000077343750$, values of $m$ at nodes near $\rho = 0$ are negative. Since Equations 2 no longer make sense for negative $m$, an interval around $\rho = 0$ has essentially been cut out. This would of course correspond to the view that pinching creates two independent geometric bodies, as suggested in Figure 9. Our single coordinate $\rho$ should then be replaced
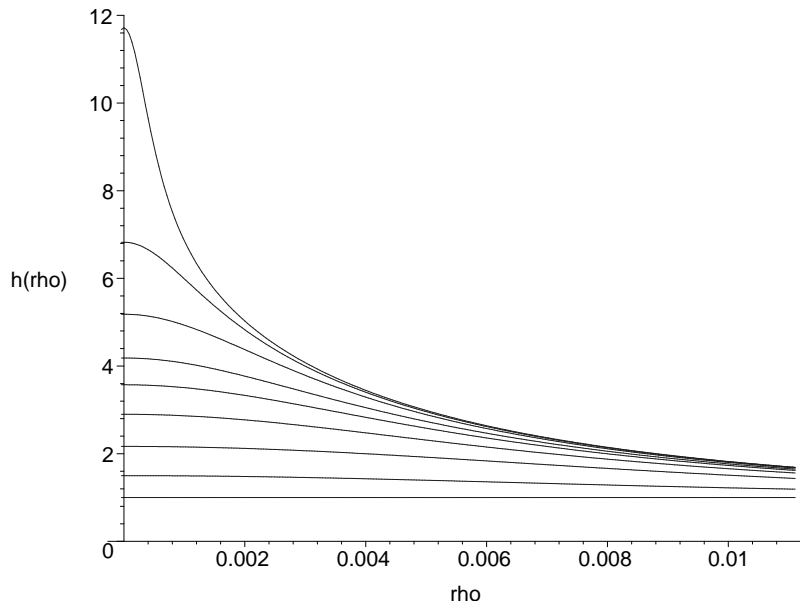
Figure 7: Qualitatively correct evolution of the metric component $g_{11} = h(\rho)$ of a 3-manifold of revolution under Ricci flow. The curves have been plotted at unequal time intervals.

by two new coordinates, one for each body, and values of $\rho$ which can no longer be attributed to the one or the other body should then be discarded as being "non-geometric". It is indeed interesting to consider what might happen *after* pinching, retaining the coordinate $\rho$ and dropping the condition that the metric should be positive definite. It is however important to note that the negative values of $m$ seen in our qualitative numerical results cannot be trusted, since they are an artifact of Euler's method being applied with a step-size so large that a singularity was passed over. What we do claim is that the cross-sections plotted in Figure 9 do still have some meaning, if one does not attempt to read anything into the missing points at the caps of the two bodies which resulted from pinching.

We return to this question in Section 6 from another point of view.

### 5.2.2  Asymptotic Scaling

A second approach to studying pinching involves series expansions of the metric components $h$ and $m$. We have expanded them to tenth order in $\rho$ (even terms only) and first order in $t$:

$$h(\rho, t) = \sum_{i=0}^{10} (h_i + \dot{h}_i\, t)\, \rho^i \quad \text{and} \quad m(\rho, t) = \sum_{i=0}^{10} (m_i + \dot{m}_i\, t)\, \rho^i.$$

Substituting into Equations (9) and (10) we get, by equating coefficients (and assuming higher-order terms are zero) equations for the quantities $\dot{h}_i$ and $\dot{m}_i$. These equations are quite cumbersome. We have used Maple [12] both to derive the equations and also to generate C code [15] to allow us to compute the flow as rapidly as possible. The C code
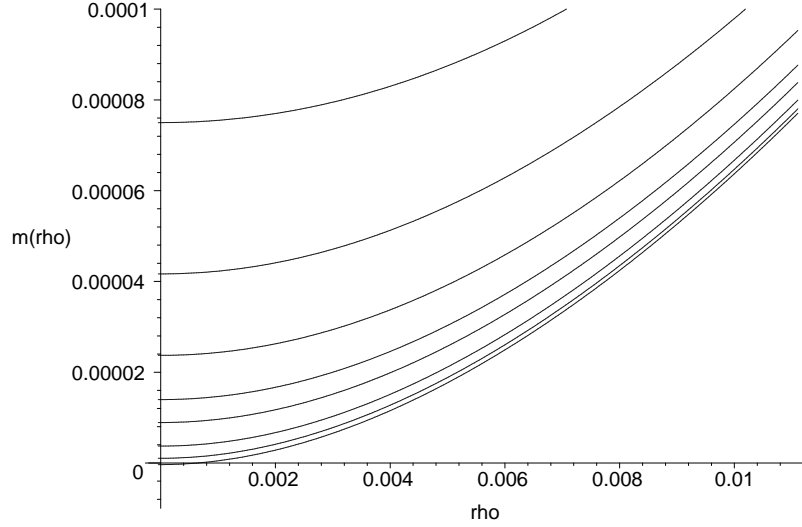
14

Figure 8: Qualitatively correct evolution of the metric component $g_{2\,2} = m(\rho)$ of a 3-manifold of revolution under Ricci flow. The curves have been plotted at unequal time intervals.

was modified to utilize the `long double` numerical data type, and the code was run on a DEC alpha (the name of a RISC microprocessor) machine with true 64 bit floating-point arithmetic (the `long double` type). We used Euler's method with a very primitive form of adaptive step-size estimation, finding these to be satisfactory for our purposes.

Our data are consistent with the qualitative results of the previous section.

We are able to use these series expansions to make some conjectures concerning the behaviour of various quantities as $t$ approaches $T$. The following scaling laws are purely empirical. They are the result of curve-fitting to the data we have, in particular for the seven points, at $t = 0.000079300, 0.000079310, 0.000079320, 0.000079330, 0.000079340,$ $0.000079345$ and $0.000079350$. The step-sizes used were significantly shorter than the differences between the times of these representative points. Figures 10 and 11 illustrate this fitting process. It is clear from these illustrations that what we believe to be asymptotic behaviour sets in fairly late. One may of course ask if we have fitted to data which is late enough in the flow to truly warrant being called asymptotic. At this stage, we can only present the data we have.

All of the following apply to $\rho = 0$:

$$
\begin{aligned}
m &\approx 1.409 \times (0.0000793514 - t)^{\phantom{-}0.985} \\
h &\approx 1.705 \times (0.0000793529 - t)^{-0.235} \\
R &\approx 0.570 \times (0.0000793515 - t)^{-1.025} \\
K(a,b) &\approx -1.142 \times (0.0000793513 - t)^{-0.826} \\
K(b,c) &\approx 0.698 \times (0.0000793514 - t)^{-0.986}
\end{aligned}
\tag{15}
$$

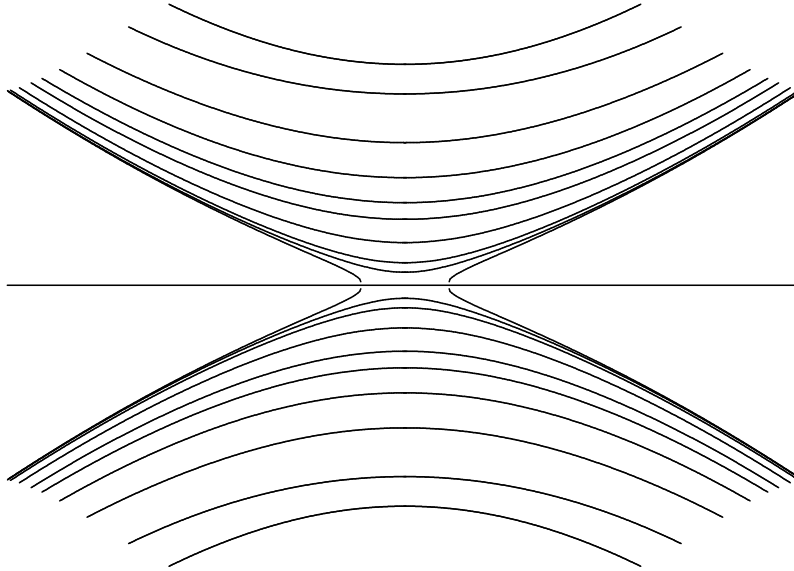It would therefore appear that $T \approx 0.0000793514$.

15

Figure 9: Qualitatively correct deformation of the cross-section of a 3-manifold of revolution under Ricci flow. The axis of rotation is horizontal. The pictures have been taken at unequal time intervals.

Note that this curve-fitting problem is ill-conditioned, although Figure 11 does suggest that our fits are as accurate as one could hope for. However, $h$ appears to diverge at a significantly later time than our estimate for $T$, and we do not find that our curves of best fit for $m$ and $K(b,c)$ obey $m \times K(b,c) = K_2$ exactly at $\rho = 0$.

We do find that the second derivative of the cross-section $y(x)$ (see Equations 2) at $x = 0$ diverges as $t \to T$, indicating that the neck becomes sharper rather than longer as the surface approaches pinching. This makes sense, since at $t = T$ we expect to have two abutting caps, as illustrated in Figure 9.

These results need to be reproduced independently (perhaps via the DeTurck flow [10]) to ascertain their validity. We present them on an "as is" basis, freely admitting that we are not even in a position to give an error analysis, but in the hope that even such preliminary data may inspire or support some new analytical attack.

It is perhaps appropriate to quote Kenkō at this point (from essay 82 of [14]):

> Leaving something incomplete makes it interesting, and gives one the feeling that there is room for growth. Someone once told me, "Even when building the imperial palace, they always leave one place unfinished."

One is tempted to think of level set methods (see [20] for a general introduction) as a possible computational alternative to what we have tried. Level set methods have been successfully applied to mean-curvature flow [6], and indeed their strength lies in their ability to cope naturally with changes in topology of an evolving surface, as pinching involves.
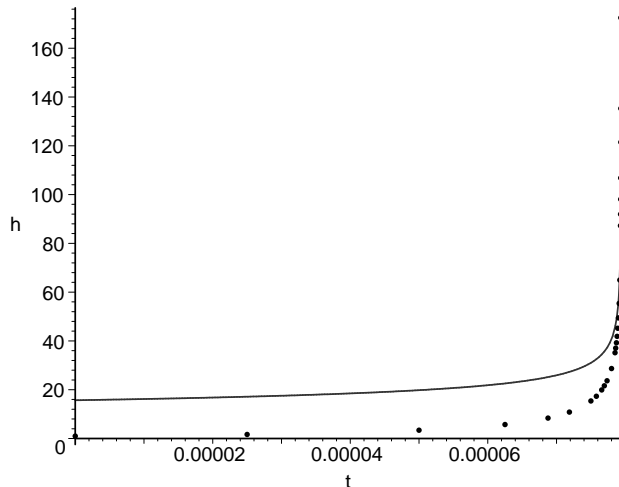
16

Figure 10: The evolution of $h$ with time for a 3-manifold of revolution. The points are numerical data. The curve is a fit to the asymptotic behaviour of $h$ near pinching.

We feel that some reformulation of the problem, perhaps along the lines of what follows, may facilitate a level set formulation of Ricci flow, and that this is without doubt a worthwhile focus for further work.

# 6 Speculation

The system of differential equations (9) and (10) above makes sense when the metric tensor is not necessarily positive definite, so long as smoothness occurs at points where $m = 0$. So we are lead to speculate about the idea of Ricci flow in the larger space of positive definite *and* indefinite metrics.

The advantage of such an approach might be that instead of the manifold pinching, one might allow that part of the manifold has a positive definite metric and part has an indefinite metric, after a singularity occurs. In this case, the computational problem might become more tractible. The reason is that the flowing family of indefinite metrics would always have a fixed domain of definition.

In particular, at a neck pinch, the initially Riemannian metric for a rotationally symmetric sphere should "jump" to a metric with a positive definite part on two polar caps and an indefinite part on an equatorial band. The indefinite part will expand and the positive definite parts contract until the metric on the whole space becomes indefinite. Further numerical experimentation might give a better idea of a suitable formulation for this process.

Note that Perelman [18] has indicated how his notion of entropy can be used as a potential function for Ricci flow. Extending this approach to the larger domain of positive definite and indefinite metrics may lead to a true level set formulation of Ricci flow, in this space of metrics on a fixed manifold. Note that at singularities where some components of
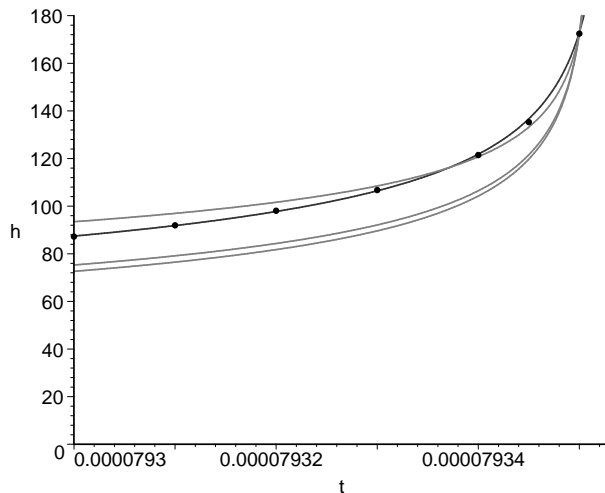
Figure 11: The evolution of $h$ with time for a 3-manifold of revolution close to pinching. The points are numerical data. The dark curve is the fit $1.705 \times (0.0000793529 - t)^{-0.235}$. The lighter curves correspond to other attempts at curve-fitting, in particular in an attempt to match the pinching time of $T = 0.0000793514$. These are $1.294 \times (0.0000793514 - t)^{-0.24}$, $1.586 \times (0.0000793514 - t)^{-0.23}$, and $5.389 \times (0.0000793514 - t)^{-0.17}$.

the Ricci tensor become infinite, one would expect the level sets to fatten ( see e.g. [1]).

# References

[1] S. Altschuler, S. Angenent and Y. Giga, *Mean curvature flow through singularities for surfaces of revolution*, The Journal of Geometric Analysis, Volume 5. 293–358 (1995).

[2] S. Angenent and D. Knopf, *An example of neck pinching for Ricci Flow on $S^{n+1}$*, to appear in Mathematical Research Letters (2004).

[3] S. Bleiler and C. Hodgson, *Spherical space forms and Dehn filling*, Topology, Volume 35, 809–833, (1996).

[4] G.L. Browning, J.J. Hack and P.N. Swartztrauber, *A Comparison of Three Numerical Methods for Solving Differential Equations on the Sphere*, Monthly Weather Review, Volume 117, 1058–1075, (1989).

[5] H. Cao, B. Chow, S. Chu and S.T. Yau, Editors, *Collected Papers on Ricci Flow*, Series in Geometry and Topology, Volume 37, International Press, MA (2003).

[6] D.L. Chopp and J.A. Sethian, *Flow under Curvature: Singularity Formation, Minimal Surfaces, and Geodesics*, Experimental Mathematics, Volume 2 (1993) 235–255.

[7] B. Chow, *The Ricci Flow on the 2-Sphere*, in H. Cao et al., Editors, *Collected Papers on Ricci Flow*, Series in Geometry and Topology, Volume 37, International Press, MA (2003) 226–237.

[8] B. Chow and D. Knopf, *The Ricci Flow: An Introduction*, Mathematical Surveys and Monographs, Volume 110, AMS (2004).

[9] M. Engman, *A Note on Isometric Embeddings of Surfaces of Revolution*, American Mathematical Monthly, Volume 111 (2004) 251–255.

[10] D. Garfinkle and J. Isenberg, *Critical behavior in Ricci flow*, arXiv:math.DG/0306129.

[11] M. Gromov and W. Thurston, *Pinching constants for hyperbolic manifolds*, Invent. Math. Volume 89, 1–12, (1989).

[12] A. Heck, *Introduction to Maple*, Third Edition, Springer-Verlag, New York, (2003).

[13] T. Ivey, *The Ricci Flow on Radially Symmetric $R^3$*, Comm. in P.D.E., Volume 19, 1481–1500, (1994).

[14] D. Keene, Translator, *Essays in Idleness: The Tsurezuregusa of Kenkō*, Columbia University Press, New York (1998).

[15] B.W. Kernighan and D.M. Ritchie, *The C Programming Language*, Second Edition, Prentice Hall, New Jersey (1988).

[16] P.R.A. Leviton and J.H. Rubinstein, *Deforming Riemannian Metrics on the 2-Sphere*, in L. Simon and N.S. Trudinger, Editors, *Miniconference on Geometry and Partial Differential Equations (Canberra 1985)*, Proceedings of the Centre for Mathematical Analysis ANU, Volume 10, Australian National University, Canberra (1986) 123–127.

[17] OpenGL Architecture Review Board et al., *OpenGL Programming Guide*, Fourth Edition, Addison-Wesley, MA (2003).

[18] G. Perelman, *The Entropy Formula for the Ricci Flow and its geometric applications*, arXiv:math.DG/0211159.

[19] G. Perelman, *Ricci Flow with surgery on three-manifolds*, arXiv:math.DG/0303109.

[20] J.A. Sethian, *Level Set Methods*, Cambridge Monographs on Applied and Computational Mathematics Vol 3, Cambridge University Press, Cambridge (1996).

[21] M. Simon, *A class of Riemannian manifolds that pinch when evolved by Ricci flow*, Manuscripta Math. Volume 101, 89–114, (2000).